COMPUTATIONAL ANALYSIS OF THE YIELD STRESS OF ULTRA-HIGH STRENGTH ALL-WELD METALS

D. ZÜGNER*+, S. HOLLY**, W. ERNST***, R. SCHNITZER**** and E. KOZESCHNIK*

** Institute of Materials Science and Technology, TU Wien, 1060, Vienna, Austria*
*** voestalpine Böhler Welding Austria GmbH, 8605, Kapfenberg, Austria; now at: voestalpine Wire Technology GmbH, 8600, Bruck an der Mur, Austria*
**** voestalpine Stahl GmbH, 4020, Linz, Austria*
***** Department of Physical Metallurgy and Materials Testing, Montanuniversität Leoben, 8700, Leoben, Austria*
+ corresponding author, dominik.zuegner@tuwien.ac.at

DOI 10.3217/978-3-85125-615-4-13

ABSTRACT

Lightweight constructions providing a high yield stress play a crucial role in transportation systems and steel constructions optimized for low energy consumption. For the fabrication of such components, the development of matching welding consumables is an essential task. In this investigation, the aim is to understand the influence of different alloying elements on the strength of all-weld metal samples of ultra-high strength filler metals with a yield strength of 1100 MPa. In the end, this should provide insight into the operating mechanisms providing the desired strength and make it possible to predict the expected yield stress with reasonable accuracy.
Apart from precipitation and solid solution strengthening, special attention is paid to the contributions of dislocation hardening and grain boundary strengthening, since these are expected to be the major contributors to the overall strength in a predominantly martensitic structure. In order to apply those classical strengthening mechanisms to the specific microstructure of martensite, additional considerations have to be made concerning the effective grain size and initial dislocation density used for calculation. Finally, the developed model is tested and the results are compared with over 90 actually produced and measured alloys.

Keywords: yield strength, welding, simulation

INTRODUCTION

In today's world there is an ever growing need for high strength materials in order to fulfil the demand for lightweight, energy-saving constructions. With this arises a need for high-strength filler materials to join those metals. Up until now, those filler metals are available with a yield strength of up to 960 MPa and the aim of the project was to develop a new material that can provide a yield strength of at least 1100 MPa. Since the process of producing flux cored wire samples, fabricating all-weld-metal samples and mechanically

testing them can be rather cumbersome, consuming both time and funds, thermokinetic simulations are employed to assess the achievable yield strength.

The simulation itself is carried out using the software package MatCalc and is split into two major parts. The first part is the simulation of the solidification process using the Scheil-Gulliver method, which not only yields the fraction but also the chemical composition of all phases that form during this early stage. These results are then transferred to the second part of the simulation, which is a complete thermokinetic simulation considering precipitation kinetics, grain size and dislocation density evolution under the given heat treatment which has been recorded during the welding process. These microstructural parameters are then used to calculate the overall yield strength of the material by employing the four classical strengthening mechanisms of grain size strengthening, dislocation strengthening, solid solution strengthening and precipitation strengthening. Considerations have been made to account for the effective grain size and dislocation density in the case of a martensitic microstructure. These simulations are then compared with over 90 different alloys that actually have been produced, welded and tested.

STATE OF THE ART

The plastic deformation of metals is dependent on the movement of dislocations throughout the material and there are various mechanisms at work that interact with these movements in one way or another. Besides the intrinsic strength of the perfect lattice, there are usually four individual strengthening mechanisms: solid solution strengthening (τ_{ss}), grain refinement (τ_{gb}), dispersion (or precipitation) strengthening (τ_{p}) and work (or dislocation) hardening (τ_{disl}). In the following sections, consideration is given to each of these strengthening mechanisms and their ability to increase the applied stress required for the onset of plastic deformation.

SOLID SOLUTION STRENGTHENING

According to Bhadeshia and Honeycombe [1], misfitting solute atoms can interfere with the motion of dislocations by the strain fields they create around them and this mechanism is called solid solution strengthening. Substitutional alloying elements (e.g. silicon, manganese) cause local expansions or contractions in the lattice. These are isotropic strains and thus they only interact with the hydrostatic components of the strain fields of dislocations.

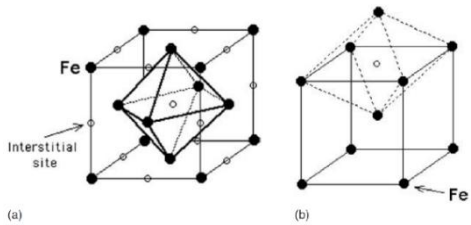

Fig. 1 (a) The regular octahedron interstice in austenite. (b) Octahedral interstice in ferrite - notice that two of the axes are longer than the third (vertical axis). This leads to a tetragonal distortion when the site is occupied by carbon [1].

Whereas interstitial atoms located at the irregular octahedron interstices in the ferritic structure cause a tetragonal distortion (Figure 1) that has a strong interaction with the shear stress, which is the dominant component of a dislocation strain field. In this lies the main reason, why interstitial solid solution strengthening is so much more potent in ferrite. The corresponding interstitial site in the austenite structure is the regular octahedron. An interstitial atom in austenite therefore acts like a substitutional element, providing only hydrostatic strain in the nearby area. This is why carbon is much less effective in strengthening austenite.

Like described by Hornbogen and Warlimont [2], because of the different sizes and other atomic parameters of the solute atoms, local strain fields are introduced to the lattice which can effectively increase the resistance to plastic deformation. The effect of atomic size differences, commonly expressed by an atomic misfit parameter δ is defined as

$$\delta = \frac{1}{a}\frac{da}{dc}, \tag{1}$$

where a is the lattice constant and c is the concentration of the solute atom in the matrix. Analogously, the shear modulus effect can be expressed as

$$\eta = \frac{1}{G}\frac{dG}{dc}, \tag{2}$$

where G is the shear modulus. To determine the strength increase by solid solution strengthening, the general formulation

$$\Delta\tau_{ss} \sim \left(\sqrt{\delta^2 + \eta^2}\right)^m \cdot c^n \tag{3}$$

may be used. In equation (3), m is an interaction exponent between 1 and 2 ([2], [3]) and n a concentration exponent, generally between 1/2 and 1 [2–9] depending on the solute concentration and temperature [6]. In literature [10–15], it is also found that the first term in equation (3) containing the atomic misfit parameter δ as well as the modulus mismatch parameter η and the exponent m is replaced by a constant strengthening coefficient k which only depends on the solute element itself and the lattice (bcc/fcc) it is dissolved in. Therefore equation (3) reduces to

$$\Delta\tau_{ss} = k \cdot c^n . \tag{4}$$

PRECIPITATION STRENGTHENING

As adequately described by Bhadeshia [1], in general there is more than one phase present in steel and the matrix is further strengthened by controlling the dispersion of these other phases in the microstructure – an effect called precipitation or dispersion strengthening. The most common other phases are carbides which are a result of the low solubility of carbon in α-iron. In plain carbon steel this carbide usually is Fe_3C (cementite) and it can occur in a wide range of structures, from a coarse lamellar form (pearlite), to fine rod or spheroidal precipitates (tempered steels). However in alloyed steel, the same variety of structures is observed, with the exception that usually the iron carbide is replaced by other carbides which are thermodynamically more stable. Other dispersed phases that can be encountered include nitrides and intermetallic compounds. For the case of fine particles, ideally small spheres that are randomly dispersed in the matrix, there are well-defined relationships between the yield stress and the parameters of the dispersion.

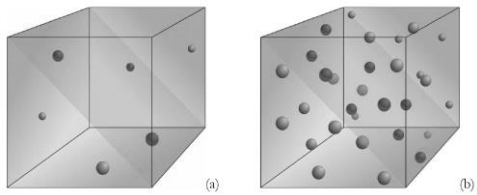

Fig. 2 Schematic illustrations of an intersected dislocation glide plane by second phase particles [16].

The effect of these densely distributed particles on the mechanical properties of the material (i.e. yield strength) is due to those precipitates acting as obstacles intersecting the glide plane of a dislocation, as can be schematically seen in Figure 2 (a) and (b). It becomes apparent that the amount of strengthening that can be achieved by dispersed second phase particles is directly related to the amount of precipitates intersecting the glide plane of a dislocation, which can be represented by the inter-particle distance. The model used for precipitations strengthening in *MatCalc* is very well described in the work of Ahmadi [17], a very simplified version of which will be outlined here.

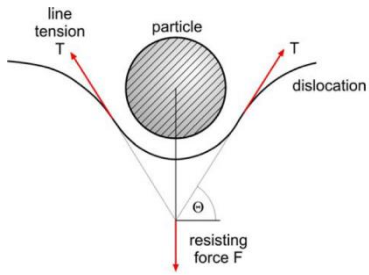

Fig. 3 General illustration of the particle-dislocation interaction. Balance of forces acting during particle resistance to dislocation movement [16].

In order to determine the absolute contribution of precipitation strengthening to the overall yield strength, the nature of the interaction between the moving dislocation and the

dispersed particles must be considered. When a single dislocation encounters a second phase particle while moving through the glide plane of a stressed metal (see Figure 3), the precipitate-dislocation interaction can be described in the most general form as

$$F = 2T \sin \Theta \,, \tag{5}$$

where T is the line tension of the dislocation section and F is the resistance force of the dispersed particle [18]. With increasing resistance force F, the dislocation gets bowed more or in other words Θ increases. In dependence of the strength of the second phase particles characterized by the resistance force F, two major cases of particle-dislocation interaction can be determined - hard and weak particles [16].

The dislocation line tension (per unit length of dislocation) has been calculated by Cottrell [19] and Foreman [20] as

$$E(\theta) = \frac{Gb^2}{4\pi}\left(\frac{1-\upsilon(\cos\theta)^2}{1-\upsilon}\right)\ln\left(\frac{r_o}{r_i}\right), \tag{6}$$

where G is the shear modulus, θ is the angle between the dislocation line and its Burgers vector, b is the magnitude of the Burgers vector, υ is Poisson's ratio and r_o, r_i is the outer and inner cut-off distance respectively [17]. Ahmadi finally formulates the line tension as

$$T(\theta) = \frac{Gb^2}{4\pi}\left(\frac{1+\upsilon-3\upsilon(\sin\theta)^2}{1-\upsilon}\right)\ln\left(\frac{r_o}{r_i}\right). \tag{7}$$

For the case of shear-able particles, the shear stress can then be formulated as

$$\tau = \frac{2T(\theta)}{bL_s}\left(\frac{F_m}{2T(\Theta)}\right)^{\frac{2}{3}}, \tag{8}$$

with L_s being the surface to surface distance between two precipitates along the dislocation, and F_m is the maximum resistance force of the precipitate in different mechanisms. And for the case of non-shear-able precipitates, the shear stress can be written as

$$\tau_{\text{Orowan}} = \frac{JGb}{2\pi\sqrt{1-\upsilon}L_s}\ln\left(\frac{2r_s}{r_i}\right), \tag{9}$$

where J is a correction constant for random arrangement of particles instead of ordered, periodic arrangement (=0.8 or 1) and r_s is the equivalent radius of the precipitate in different models. For a more detailed and complete description of the model please refer to [17], [21], [22].

The mechanisms that contribute to strengthening include coherency strengthening, which arises from the coherency strains developed in the matrix around a coherent particle, chemical hardening, which relates to the development of antiphase boundaries when a dislocation cuts through a precipitate, and dispersion hardening, which arises from looping of the dislocation between hard non-deformable particles as described by Orowan [23].

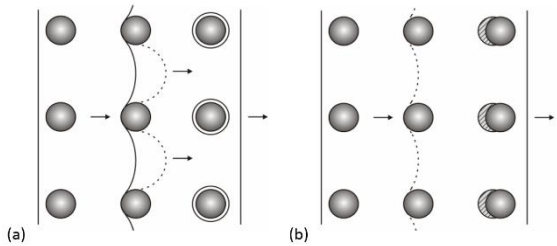

Fig 4 Particle-dislocation interaction for hard (a) and weak (b) particles [16].

Holzer [16] summarizes the two cases described by Ahmadi [17] as follows. If the strength (i.e. the resistance force F) of the dispersed particle exceeds twice the line tension of the dislocation ($F \geq 2T, \Theta = 90°$), the particle will not be cut through or sheared by the dislocation. Therefore the obstacle is denoted as a strong particle. In this case, the dislocation may bypass the precipitate either by the Orowan mechanism or cross slip. The second phase particle will remain unchanged, namely non-deformed (Figure 4 (a)), thus the properties of the precipitate will not affect the amount of precipitation strengthening exerted by it. In contrary if the precipitates are weak ($F < 2T, \Theta < 90°$) and therefore sheared by the dislocation, the particle will deform as can be seen schematically in Figure 4 (b). In this case the properties of the second phase particles will strongly affect the amount of precipitation strengthening and numerous effects may be involved in raising the stress required for yielding related to phenomena like chemical strengthening, coherency strengthening or modulus mismatch hardening.

GRAIN BOUNDARY STRENGTHENING

For a basic description of the effect of grain size refinement of ferrite, which represents one of the most important strengthening routes in the heat treatment of steel, we will resort to the work of Bhadeshia [1] once more. The first scientific analysis of the relationship between grain size and strength, performed by Hall and Petch, led to the famous Hall-Petch relationship between the grain diameter d and the yield stress σ_y,

$$\sigma_y = \sigma_0 + k_y d^{-\frac{1}{2}}, \tag{10}$$

where σ_0 and k_y are constants. This type of relationship has been confirmed to be appropriate for a wide range of steels as well as for many non-ferrous metals and alloys. The term σ_0 is called friction stress and it represents the stress required to move free dislocations along the slip planes in the bcc crystals, and can also be seen as the yield stress of a single crystal ($d^{-\frac{1}{2}} = 0$). This friction stress is particularly sensitive to temperature and chemical composition. The constant k_y represents the slope of the σ_y-$d^{-\frac{1}{2}}$ plot which has been found to be insensitive to temperature, chemical composition and strain rate. In agreement with the Cottrell-Bilby theory of the yield point involving the unsnapping of dislocations from interstitial carbon atmospheres, k_y has been referred to as the unpinning parameter. Nevertheless, the fact that k_y is not sensitive to temperature suggests that unpinning rarely occurs, and emphasizes the theory that new dislocations are generated at

the yield point. That statement is consistent with the theories that explain the yield point in terms of the movement of new dislocations, the velocities of which are stress dependent.

For the strength contribution by grain refinement in the case of all weld metals, which in our case consist of a primarily martensitic microstructure, attention has to be paid to what effective grain size is used for the Hall-Petch relationship. There is a strong relationship between the prior austenite grain size and the hierarchical microstructure of lath-martensite (Figure 5) as reported by Galindo-Nava et al. [24]. The interesting conclusion concerning this relationship will be outlined in the following.

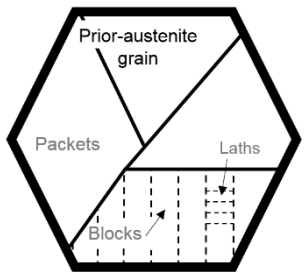

Fig. 5 Hierarchical microstructure of martensite. The prior austenite grains contain packets, which consist of blocks of laths [24].

Martensite packets are formed by laths sharing a common habit plane, with four possible variants of the $\{1\,1\,1\}_\gamma$ planes in the Kurdjumov-Sachs (K–S) relation, the number of packets per austenite grain is equal to $N_p = 4$. Additionally the strain controlling the martensitic transformation is composed by a dilatation, remaining constant for each K–S relation, and a shear strain differing from each variant [25]. This means that all six lath orientation variants in a given packet should be present in order to minimize the elastic energy and decrease the overall strain. This indicates that the possible number of blocks per packet should be $N_b = 6$ [24]. Combining these results the packet and block size in dependence of the austenite grain diameter (D_g) should be equal to

$$\begin{aligned} d_{\text{packet}} &= \sqrt{\frac{3\sqrt{3}}{8N_p}}D_g = \sqrt{\frac{3\sqrt{3}}{32}}D_g = 0.40D_g\,, \\ d_{\text{block}} &= \frac{1}{N_b}d_{\text{packet}} = \frac{1}{6}d_{\text{packet}} = 0.067D_g. \end{aligned} \tag{11}$$

We used an effective block size of $0.067D_g$ in accordance with equation (10) upon the transformation to martensite for our calculations.

DISLOCATION STRENGTHENING

Strengthening by dislocation represents another very important route when trying to increase the strength of steel, bearing a tremendous potential. In fact, plain carbon steel can

be raised to strength levels above $1500\ \mathrm{Nm}^{-2}$, without the addition of special alloying elements, simply by the phenomenon of work hardening [1]. Despite the fact that the weld joint is not subjected to any external mechanical deformations, the transformation to the martensitic structure introduces internal stress and deformation and therefore work hardening or dislocation strengthening can and should not be neglected.

The strength increase by dislocation hardening can be determined according to the formulation of Taylor ([13], [26], [27])

$$\tau_{\mathrm{disl.}} = \alpha \cdot G \cdot b \cdot \sqrt{\rho}\,, \tag{12}$$

where the strength contribution τ_{disl} is a function of the shear modulus G, the Burgers vector b, the free dislocation density ρ and α which is a constant. The initial dislocation density ρ_0 is taken from a formulation by Takahashi and Bhadeshia [28]

$$\log \rho_0 = 9.28480 + \frac{6880{,}73}{M_S} - \frac{1780360}{M_S^2}, \tag{13}$$

where M_S is the martensite start temperature in $°C$, which can also be calculated empirically using any of the available regressions, i.e. the one by Arjomandi et al. [29].

After the transformation, the dislocation density is assumed to evolve under the given heat treatment according to the approach proposed by Sherstnev et al. [30], adapted by Buken and Kozeschnik [31], that describes the rate of the total dislocation density evolution $\dot{\rho}$ as

$$\dot{\rho} = \frac{M\sqrt{\rho}}{Ab}\dot{\phi} - 2B\frac{d_{\mathrm{ann}}}{b}\rho M\dot{\phi} - 2CD_{\mathrm{Dis}}\frac{Gb^3}{k_B T}(\rho^2 - \rho_{\mathrm{RS}}^2), \tag{14}$$

with the Taylor factor M, the Burgers vector b, the critical dislocation annihilation distance d_{ann}, the substitutional self-diffusion coefficient at dislocations D_{Dis}, the strain rate $\dot{\phi}$, the amount of geometrically necessary dislocations ρ_{RS} and material parameters A, B and C.

SCHEIL GULLIVER ANALYSIS

Primary precipitates are particles that form during the solidification process of the weld metal. They are usually of rather large size and do not participate in any further reactions, therefore it is assumed that they do not significantly contribute to dispersion strengthening. However their formation does alter the chemical composition of the remaining material thus they should be taken into account.

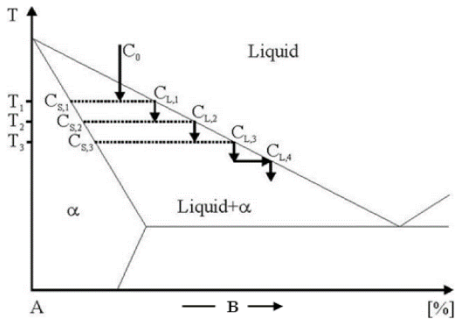

Fig. 6 Scheme of Scheil solidification of a hypothetic Fe-C alloy. During solidification the actual liquid phase, beginning with C_0, is undercooled and solidifies according to the lever rule enriching the liquid phase with solute atoms [32].

By employing the Scheil-Gulliver analysis, it is possible to calculate the fraction and composition of all phases during solidification step by step from the liquidus temperature to the temperature where solidification of the residual liquid phase occurs [33]. The residual liquid fraction at final solidification depends on the cooling rate. Higher cooling rates in general lead to higher fractions, whereas low rates of cooling enable the liquid film to become very thin and the residual liquid enriches more than in the case of higher fraction residual liquid at solidification. Figure 6 schematically shows how the Scheil-Gulliver analysis is performed. Liquid metal with the initial composition C_0 is undercooled which leads to a local equilibrium and the formation of a solid fraction with the composition $C_{S,1}$ and a liquid fraction with the composition $C_{L,1}$ (with the ratio between liquid and solid following the lever rule). Due to their low mobility in the solid phase, the diffusion of substitutional elements is halted from this point on, but it is assumed that the interstitial elements (i.e. carbon, nitrogen and boron) are still mobile in both phases which causes back-diffusion of those atoms, striving for an equilibrium between the liquid and solid phase. Then this process is repeated with the concentration $C_{L,1}$ and so on and so forth.

EXPERIMENTAL

MATERIALS AND WELDING

All materials used for the experiments and simulations were experimental alloys that were fabricated during the development of the new filler material at the *voestalpine Böhler Welding* GmbH. To give the reader an idea as to what materials we are dealing with here, Table 1 contains approximate ranges for the content of each chemical element.

Table 1 Approximate chemical composition of all alloys.

Element	Content range in wt%
C	0.05 - 0.15
N	0.00 - 0.03
Si	0.20 - 0.80
Mn	0.80 - 2.10
P	0.00 - 0.01
Cr	0.11 - 0.98
Mo	0.00 - 0.78
Ni	0.99 - 3.20
Nb	0.00 - 0.07
V	0.10 - 0.34
W	0.00 - 0.02
Cu	0.00 - 0.81
Co	0.00 - 0.35
Ti	0.00 - 0.11
As	0.00 - 0.01
Sn	0.00 - 0.01
Zr	0.00 - 0.01
Sb	0.00 - 0.01
B	0.00 - 0.01
Al	0.00 - 0.01

As described in other publications within this project ([34] and [35]), numerous metal-cored wires with different chemical compositions were produced and samples were welded. All-weld metal samples were prepared in accordance with EN 15792-1 in position PA using Ar + 18 % CO_2 as shielding gas. They were fabricated with eight weld passes, each consisting of three beads. The welding parameters are shown in Table 2. S235 was used as base material and three layers were applied as buffer.

Table 2 Welding parameters used.

Current [A]	Voltage [V]	Welding speed [mm/min]	Heat input per unit length [kJ/mm]	Interpass-temperature [°C]
250	26.5	550	0.71	150

MECHANICAL TESTING

The welded samples for mechanical testing were subjected to a soaking heat treatment at 150°C for 16 h according EN ISO 15792-1. Tensile and charpy V impact toughness testing were performed on all-weld samples. The tensile tests were carried out on single specimens and were done at ambient temperature in accordance to EN ISO 6892-1. The impact tests were conducted on three samples in order to get a set of statistics. Impact tests of samples were performed at ambient temperature and -20°C defined by EN ISO 9016. See also [34].

SIMULATION

THERMOKINETIC CALCULATIONS USING MATCALC

All simulations were conducted using the thermokinetic software package *MatCalc* ([36], [37]), version 6.00.0218, utilizing CALPHAD-type [38] Gibbs energies (database: 'mc_fe.tdb') to calculate chemical potentials, driving forces for precipitation and interfacial energies. A script is used for all calculations, performing a Scheil-Gulliver analysis for the solidification process followed by a precipitation kinetics simulation under the given heat treatment which can be seen in Figure 7. The peaks of reheating after the initial cooling are due to the passing of additional weld beads. This temperature evolution has been recorded with a thermocouple placed within the first welding seam.

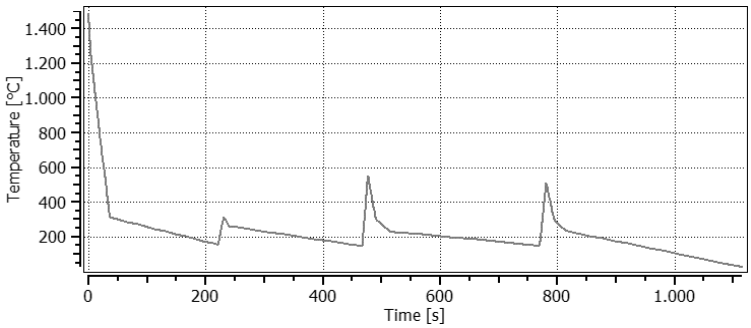

Fig. 7 Evolution of temperature used for simulations in *MatCalc*.

The individual strength contributions, namely solid solution strengthening (τ_{ss}), grain refinement (τ_{gb}), dispersion (or precipitation) strengthening (τ_p), work (or dislocation)

hardening (τ_d) and intrinsic lattice strength (τ_i) are summed up in *MatCalc* in the following way

$$\tau = (\tau_A^{\alpha} + \tau_B^{\alpha})^{\frac{1}{\alpha}}, \tag{15}$$

where τ_A equals τ_d and $\tau_B = \tau_i + \tau_{ss} + \tau_p + \tau_{gb}$. The factor α is set to a value of 1.8.

The parameters used for the simulation, including values for solute drag and others are summarized in Table 3. Additional settings include activated back-diffusion for carbon, nitrogen and boron during Scheil calculation, phases include AlN, cementite and composition sets for TiN, TiC, NbN, NbC and VCN, for evolution of grain size the multi-class model was used. The amount of primary precipitates is directly imported from the Scheil calculation.

Table 3 Parameters used for the MatCalc simulation.

Parameter	Value	Unit	Description
$T_{S,s}$	**1600**	$°C$	Starting temperature for Scheil analysis
$T_{S,f}$	**1000**	$°C$	Finish temperature for Scheil analysis
$T_{S,St}$	**1.0**	$°C$	Step value for Scheil analysis
$f_{res.liq.}$	**0.03**	$-$	Residual liquid fraction at which to stop Scheil
$r_{prim.}$	**600E-9**	m	Radius of primary precipitates from Scheil
D_γ	**10E-6**	m	Starting grain diameter for austenite
$V_{mis.,Cem.}$	**0.01**	$-$	Volumetric misfit of cementite
$V_{mis.,NbC}$	**0.1**	$-$	Volumetric misfit of NbC
$V_{mis.,NbN}$	**0.1**	$-$	Volumetric misfit of NbN
$V_{mis.,TiC}$	**0.05**	$-$	Volumetric misfit of TiC
$V_{mis.,TiN}$	**0.05**	$-$	Volumetric misfit of TiN
$V_{mis.,AlN}$	**0.27**	$-$	Volumetric misfit of AlN
$V_{mis.,VCN}$	**0.03**	$-$	Volumetric misfit of V[C,N]
$T_{crit.,TiN}$	**4000**	$°K$	$T_{crit.}$ for diffuse interface effect of TiN
$T_{crit.,TiC}$	**3500**	$°K$	$T_{crit.}$ for diffuse interface effect of TiC
$T_{crit.,NbN}$	**3360**	$°K$	$T_{crit.}$ for diffuse interface effect of NbN
$T_{crit.,NbC}$	**3500**	$°K$	$T_{crit.}$ for diffuse interface effect of NbC
$T_{crit.,VCN}$	**2425**	$°K$	$T_{crit.}$ for diffuse interface effect of V[C,N]
$\dot{\epsilon}_\gamma$	**1E-3**	s^{-1}	Assumed strain rate of weld joint during cooling
$A_{SLK,fcc}$	**33**	$-$	A-parameter for evolution of ρ in fcc
$B_{SLK,fcc}$	$\mathbf{-0.646 \ln \dot{\epsilon}_\gamma + 7.5}$	$-$	B-parameter for evolution of ρ in fcc
$C_{SLK,fcc}$	**5E-5**	$-$	C-parameter for evolution of ρ in fcc
$A_{SLK,bcc}$	**30**	$-$	A-parameter for evolution of ρ in bcc
$B_{SLK,bcc}$	**2**	$-$	B-parameter for evolution of ρ in bcc
$C_{SLK,bcc}$	**1e-3**	$-$	C-parameter for evolution of ρ in bcc
S_{SLK}	**33**	$-$	Similitude-parameter for evolution of ρ
k_d	**2.0**	$-$	k_d parameter for evolution of ρ
k_r	**1.5**	$-$	k_d parameter for evolution of ρ
CLS_V	**1500**	J/mol	Interaction energy for solute drag of V
CLS_{Ti}	**12000**	J/mol	Interaction energy for solute drag of Ti
CLS_{Nb}	**18000**	J/mol	Interaction energy for solute drag of Nb
CLS_{Mo}	**9000**	J/mol	Interaction energy for solute drag of Mo
CLS_{Mn}	**6000**	J/mol	Interaction energy for solute drag of Mn
CLS_{Si}	**2500**	J/mol	Interaction energy for solute drag of Si
CLS_{Ni}	**3000**	J/mol	Interaction energy for solute drag of Ni
CLS_{Cr}	**3000**	J/mol	Interaction energy for solute drag of Cr

RESULTS

COMPARISON OF CALCULATED AND MEASURED VALUES

A comparison of measured and simulated values for the yield strength can be found in Figure 8.

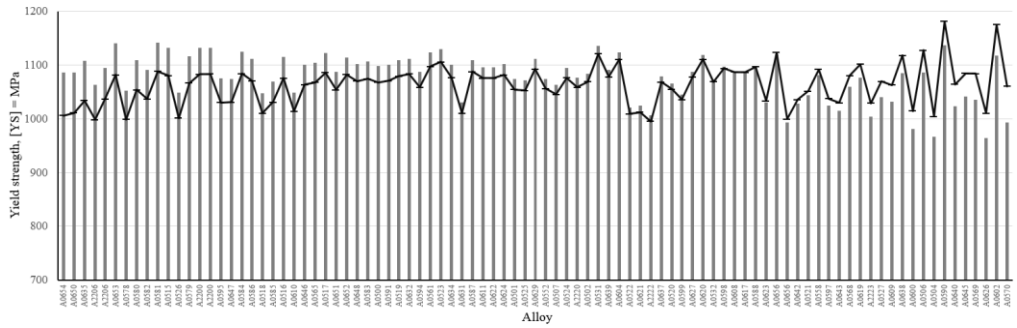

Fig. 8 Comparison of measured (bars) and calculated (line) values for the yield strength.

There was an overall good agreement between measured and calculated values, with an approximate mean deviation of 3% for the values shown in Figure 8. Although the ductility of the samples was measured, it was not simulated due to the much more complex nature of fracture.

EXEMPLARY SIMULATION RESULTS

This section shows some detailed simulation results for a selected alloy to give an impression as to how some parameters evolve during the initial cooling and reheating of the weld joint. Exemplary results for the simulation of the solidification process with the formation of primary precipitates by the means of a Scheil-Gulliver analysis are found in Figure 9.

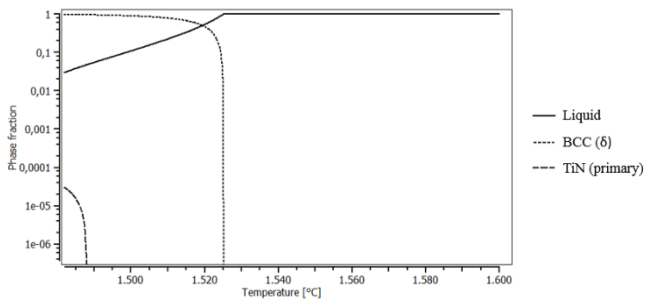

Fig. 9 Results of the Scheil-Gulliver analysis.

The only primary precipitate that forms in the investigated alloys is titanium nitride. This result is then transferred to the precipitation simulation, the results of which follow. The

simulated phase fraction of all phases with a greater fraction than 1E-8 and the evolution of temperature, in other words the heat treatment, can be seen in Figure 10. In this context, (dis) means nucleation at dislocations in the bulk and (gb) means nucleation at grain boundaries.

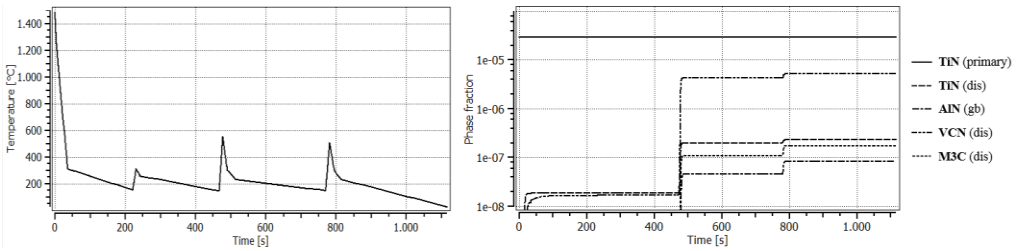

Fig. 10 Heat treatment (left) and simulated evolution of phase fractions (right).

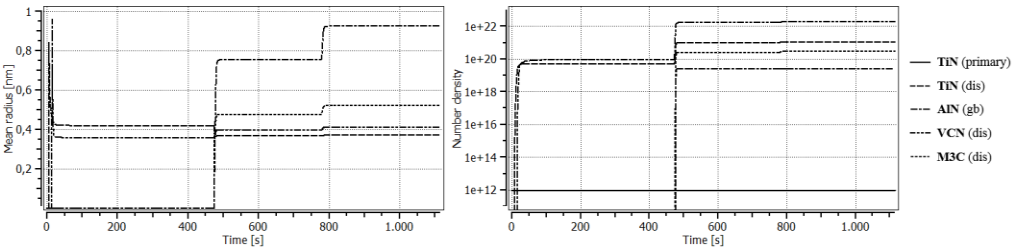

Fig. 11 Simulated mean radii of precipitates (left) and number densities (right).

For the development of the mean grain diameter within the first minute please refer to Figure 12. Please note that upon transformation to martensite (at approximately 34 seconds) the diameter switches according to equation (11).

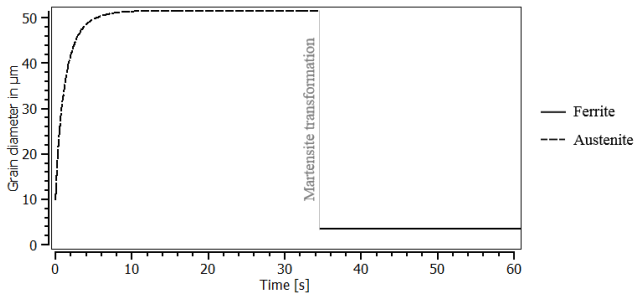

Fig. 12 Evolution of mean grain diameter in austenite (multi-class) and transformation to martensite.

Finally, the simulated evolution of the total dislocations density and the total calculated yield strength with all contributions (excluding intrinsic lattice strength – which is constant anyways) can be seen in Figure 13.

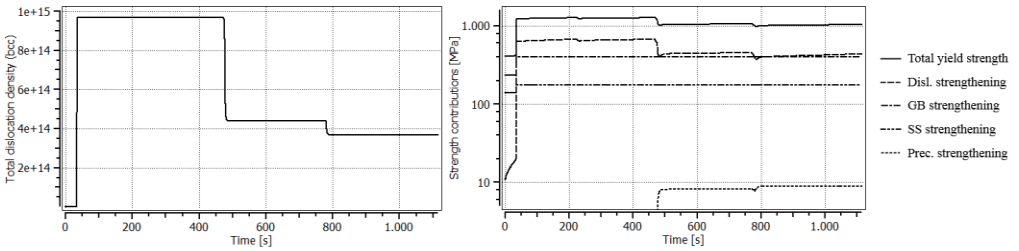

Fig. 13 Simulated total dislocation density (left) and simulated total yield with individual contributions (right).

DISCUSSION

The overall agreement of simulated values for the yield stress with the measured ones was good. However there were still some extreme outliers, some of which were not included in the evaluation and most of these can be attributed to fluctuations besides chemical composition, like deviations in the welding parameters for example. Therefore it would be advisable to employ robotic welding for fabrication of the samples in the future.

Simulations of the solidification process via the Scheil-Gulliver method have revealed that the only primary precipitates in these alloys were titanium nitride which can be explained by the low solubility product compared to other nitrides and carbides and a high affinity of titanium to nitrogen. It is assumed that those precipitates do not participate in any further reactions due to their large size and therefore their number density and phase fraction remains constant.

As for the precipitation kinetics simulations, when looking at Figure 10 it becomes apparent that especially the peaks of reheating after the initial cooling of the weld, which are due to the passing of additional weld beads in proximity to the first one, have a high impact on the outcome of the calculation. This fact can be seen in Figure 10 on right side where especially the first peak that exceeds temperatures over 500°C increases the phase fraction of certain precipitates by two to three orders of magnitude. Nevertheless we are dealing with a relatively low alloying content in these welds and a fast initial cooling rate which results in a very small precipitate size but higher number densities as depicted in Figure 11. The approach to assess the yield stress contribution of martensite by its grainsize and high dislocation density (Figure 12 and Figure 13 left) is yielding good overall results. It is noteworthy that that plateau value of the austenite grain size is not really depending on the chosen initial grain size, within reasonable boundaries of course. Obviously these two mechanisms are the dominating ones in this model, followed by solid solution strengthening and lastly precipitation strengthening (Figure 13 right). For investigations to come, additional attention should be paid to the development of the grain size and the model should be calibrated and adjusted with extensive measurements of the prior austenite grain size and the martensite block size. It might also be advisable to exclude geometrically necessary dislocations from the strength contribution by dislocation strengthening, since those are already considered by grain size strengthening.

SUMMARY AND CONCLUSION

Thermokinetic simulations using MatCalc provide a very useful tool for the development of new filler materials since they not only provide a reasonable assessment of the overall strength that can be achieved with a specific chemical composition but also provide some insight into what is happening during the welding process. It was revealed that e.g. especially the second peak of reheating has a high impact on precipitation behavior.

More work on the model is needed, backed up by experimental investigations, however the framework provided is already yielding very good results and has the potential to significantly reduce the requirement for actual manufacturing of samples in future development processes.

REFERENCES

[1] BHADESHIA, H.K.D.H. ; HONEYCOMBE, SIR ROBERT: The Strengthening of Iron and its Alloys. In: *Steels* : Elsevier, 2006 — ISBN 9780750680844, S. 17–38

[2] HORNBOGEN, ERHARD ; WARLIMONT, HANS: *Metallkunde*. Berlin, Heidelberg : Springer Berlin Heidelberg, 2001. — ISBN 978-3-662-08696-4

[3] GYPEN, L.A. ; DERUYTTERE, A.: The combination of atomic size and elastic modulus misfit interactions in solid solution hardening. In: *Scripta Metallurgica* Bd. 15 (1981), Nr. 8, S. 815–820.

[4] GOMIERO, P. ; BRECHET, Y. ; LOUCHET, F. ; TOURABI, A. ; WACK, B.: Microstructure and mechanical properties of a 2091 AlLi alloy—II. Mechanical properties: Yield stress and work hardening. In: *Acta Metallurgica et Materialia* Bd. 40 (1992), Nr. 4, S. 857–861.

[5] BUTT, M.Z. ; FELTHAM, P.: Solid-solution hardening. In: *Acta Metallurgica* Bd. 26 (1978), Nr. 1, S. 167–173.

[6] BUTT, M. Z. ; FELTHAM, P.: Solid-solution hardening. In: *Journal of Materials Science* Bd. 28 (1993), Nr. 10, S. 2557–2576.

[7] SIEURIN, HENRIK ; ZANDER, JOHAN ; SANDSTRÖM, ROLF: Modelling solid solution hardening in stainless steels. In: *Materials Science and Engineering: A* Bd. 415 (2006), Nr. 1–2, S. 66–71

[8] TRAUB, H. ; NEUHÄUSER, H. ; SCHWINK, CH.: Investigations of the yield region of concentrated CuGe and CuZn single crystals—I. Critical resolved shear stress, slip line formation and the true strain rate. In: *Acta Metallurgica* Bd. 25 (1977), Nr. 4, S. 437–446.

[9] ZANDER, JOHAN ; SANDSTRÖM, ROLF ; VITOS, LEVENTE: Modelling mechanical properties for non-hardenable aluminium alloys. In: *Computational Materials Science* Bd. 41 (2007), Nr. 1, S. 86–95.

[10] GYPEN, L. A. ; DERUYTTERE, A.: Multi-component solid solution hardening. In: *Journal of Materials Science* Bd. 12 (1977), Nr. 5, S. 1028–1033.

[11] GYPEN, L. A. ; DERUYTTERE, A.: Multi-component solid solution hardening. In: *Journal of Materials Science* Bd. 12 (1977), Nr. 5, S. 1034–1038.

[12] HUTCHINSON, C ; GOUNE, M ; REDJAIMIA, A: Selecting non-isothermal heat treatment schedules for precipitation hardening systems: An example of coupled process–property optimization. In: *Acta Materialia* Bd. 55 (2007), Nr. 1, S. 213–223.

[13] LI, Q: Modeling the microstructure–mechanical property relationship for a 12Cr–2W–V–Mo–Ni power plant steel. In: *Materials Science and Engineering A* Bd. 361 (2003), Nr. 1–2, S. 385–391.

[14] GLADMAN, T.: *The physical metallurgy of microalloyed steels*, 1997 — ISBN 0910716812

[15] YOUNG, C. H. ; BHADESHIA, H. K. D. H.: Strength of mixtures of bainite and martensite. In: *Materials Science and Technology* Bd. 10 (1994), Nr. 3

[16] HOLZER, I: *Modelling and Simulation of Strengthening in Complex Martensitic 9-12% Cr Steel and a Binary Fe-Cu Alloy*, Dissertation, TU Wien, 2010

[17] AHMADI, M.R. ; POVODEN-KARADENIZ, E. ; ÖKSÜZ, K.I. ; FALAHATI, A. ; KOZESCHNIK, E.: A model for precipitation strengthening in multi-particle systems. In: *Computational Materials Science* Bd. 91 (2014), S. 173–186

[18] GLADMAN, T.: Precipitation hardening in metals. In: *Materials Science and Technology* Bd. 15 (1999), Nr. 1, S. 30–36

[19] COTTRELL, A.H.: Theory of dislocations. In: *Progress in Metal Physics* Bd. 4 (1953), S. 205–264

[20] FOREMAN, A.J.E: Dislocation energies in anisotropic crystals. In: *Acta Metallurgica* Bd. 3 (1955), Nr. 4, S. 322–330

[21] AHMADI, M.R. ; POVODEN-KARADENIZ, E. ; SONDEREGGER, B. ; ÖKSÜZ, K.I. ; FALAHATI, A. ; KOZESCHNIK, E.: A model for coherency strengthening of large precipitates. In: *Scripta Materialia* Bd. 84–85 (2014), S. 47–50

[22] AHMADI, M.R. ; SONDEREGGER, B. ; POVODEN-KARADENIZ, E. ; FALAHATI, A. ; KOZESCHNIK, E.: Precipitate strengthening of non-spherical precipitates extended in 〈100〉 or {100} direction in fcc crystals. In: *Materials Science and Engineering: A* Bd. 590 (2014), S. 262–266

[23] Internal Stresses in Metals and Alloys. In: *Nature* Bd. 161 (1948), Nr. 4080, S. 70–71

[24] GALINDO-NAVA, E.I. ; RIVERA-DÍAZ-DEL-CASTILLO, P.E.J.: A model for the microstructure behaviour and strength evolution in lath martensite. In: *Acta Materialia* Bd. 98, Acta Materialia Inc. (2015), S. 81–93

[25] KINNEY, C.C. ; PYTLEWSKI, K.R. ; KHACHATURYAN, A.G. ; MORRIS, J.W.: The microstructure of lath martensite in quenched 9Ni steel. In: *Acta Materialia* Bd. 69 (2014), S. 372–385

[26] Focus on Recent Breakthroughs in Materials Science and Technology. In: *Science and Technology of Advanced Materials* Bd. 9 (2008), Nr. 1, S. 010301

[27] MARUYAMA, KOUICHI ; SAWADA, KOTA ; KOIKE, JUN-ICHI: Advances in Physical Metallurgy and Processing of Steels. Strengthening Mechanisms of Creep Resistant Tempered Martensitic Steel. In: *ISIJ International* Bd. 41 (2001), Nr. 6, S. 641–653

[28] TAKAHASHI, M. ; BHADESHIA, H. K. D. H.: Model for transition from upper to lower bainite. In: *Materials Science and Technology* Bd. 6 (1990), Nr. 7, S. 592–603

[29] ARJOMANDI, M. ; KHORSAND, H. ; SADATI, S.H. ; ABDOOS, H.: Prediction of martensite formation start temperature in steels using artificial neural networks. In: *Defect and Diffusion Forum* Bd. 273–276 (2008), S. 329–334

[30] SHERSTNEV, P ; LANG, P ; KOZESCHNIK, E: No Title. In: *Eur. Congr. Comput. Methods Appl.*, 2012

[31] BUKEN, HEINRICH ; KOZESCHNIK, ERNST: A Model for Static Recrystallization with Simultaneous Precipitation and Solute Drag. In: *Metallurgical and Materials Transactions A: Physical Metallurgy and Materials Science* Bd. 48, Springer US

(2017), Nr. 6, S. 2812–2818

[32] WARCZOK, PIOTR: *Simulation of solidification of 0.7C 3Mn steel*. URL http://matcalc.tuwien.ac.at/wiki/doku.php?id=tutorials:t11. - abgerufen am 2015-04-04

[33] KOZESCHNIK, E. ; RINDLER, W. ; BUCHMAYR, B.: Scheil–Gulliver simulation with partial redistribution of fast diffusers and simultaneous solid–solid phase transformations. In: *International Journal of Materials Research* Bd. 98 (2007), Nr. 9, S. 826–831

[34] HOLLY, S. ; HASLBERGER, P. ; ZÜGNER, D. ; SCHNITZER, R. ; KOZESCHNIK, E.: Development of high-strength welding consumables using calculations and microstructural characterisation. In: *Welding in the World* Bd. 62 (2018), Nr. 3, S. 451–458

[35] SCHNITZER, RONALD ; ZÜGNER, DOMINIK ; HASLBERGER, PHILLIP ; ERNST, WOLFGANG ; KOZESCHNIK, ERNST: Influence of alloying elements on the mechanical properties of high-strength weld metal. In: *Science and Technology of Welding and Joining* Bd. 22 (2017), Nr. 6, S. 536–543

[36] SVOBODA, J ; FISCHER, F D ; FRATZL, P ; KOZESCHNIK, E: Modelling of kinetics in multi-component multi-phase systems with spherical precipitates I : Theory. In: *Materials Science and Engineering A* Bd. 385 (2004), S. 166–174

[37] KOZESCHNIK, E ; SVOBODA, J ; FRATZL, P ; FISCHER, F D: Modelling of kinetics in multi-component multi-phase systems with spherical precipitates II : Numerical solution and application. In: *Materials Science and Engineering A* Bd. 385 (2004), S. 157–165

[38] LUKAS, HANS ; FRIES, SUZANA G. ; SUNDMAN, BO: *Computational Thermodynamics*. Cambridge : Cambridge University Press, 2007 — ISBN 9780511804137